



The Abdus Salam
International Centre for Theoretical Physics


United Nations
Educational, Scientific
and Cultural Organization


International Atomic
Energy Agency



SMR.1670 - 29

INTRODUCTION TO MICROFLUIDICS

8 - 26 August 2005

Chip-based IR and Raman Spectroscopy

H. Gardeniers
University of Twente, Enschede, The Netherlands

Chip-based IR and Raman spectroscopy

Han Gardeniers
MESA+ Institute for Nanotechnology
University of Twente

Summer School in Microfluidics
ICTP, Trieste, Italy



InfraRed basics

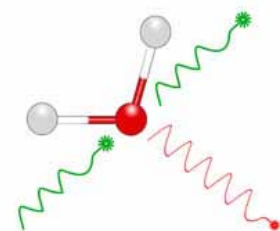
Region	Wavelength range (μm)	Wavenumber range (cm^{-1})
Near	0.78 - 2.5	12800 - 4000
Middle	2.5 - 50	4000 - 200
Far	50 - 1000	200 - 10

(wavenumber = $1 / \text{wavelength in centimeters}$)

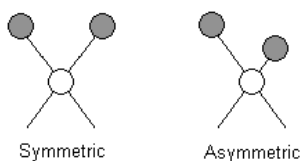
The most useful IR region is between $4000 - 670 \text{ cm}^{-1}$

IR radiation interacts with vibrational and rotational states of molecules, in case the vibrations or rotations cause a net change in the dipole moment of the molecule.

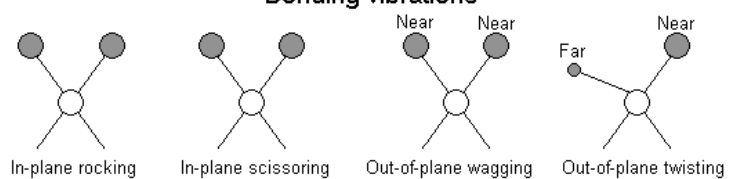
Rotational transitions are only visible for gases, in liquids or solids, the corresponding IR lines broaden into a continuum due to molecular collisions and other interactions.



Stretching vibrations



Bending vibrations



Change in inter-atomic distance along bond axis

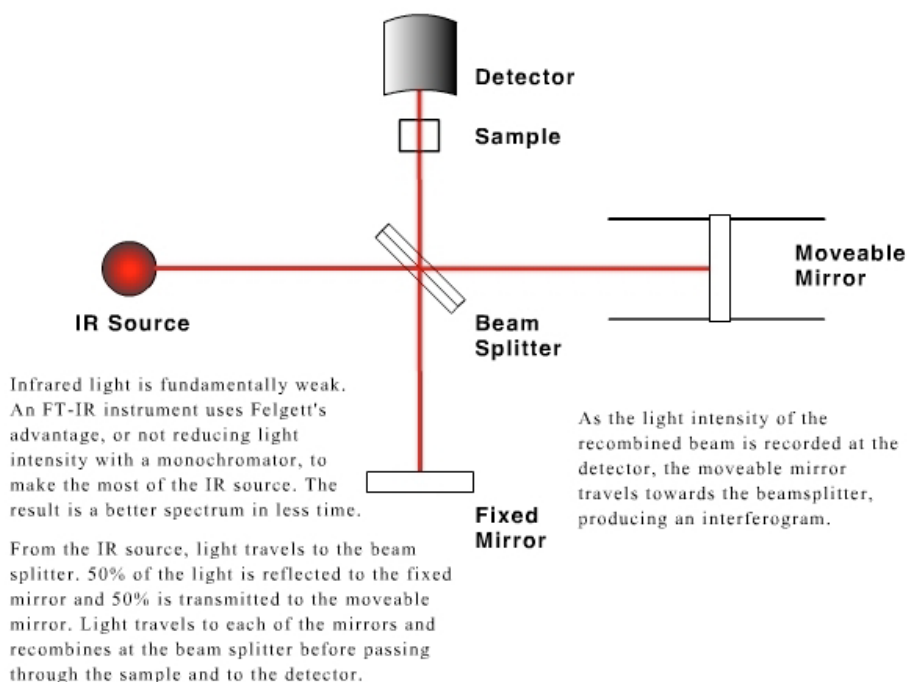
Change in angle between two bonds.

InfraRed basics

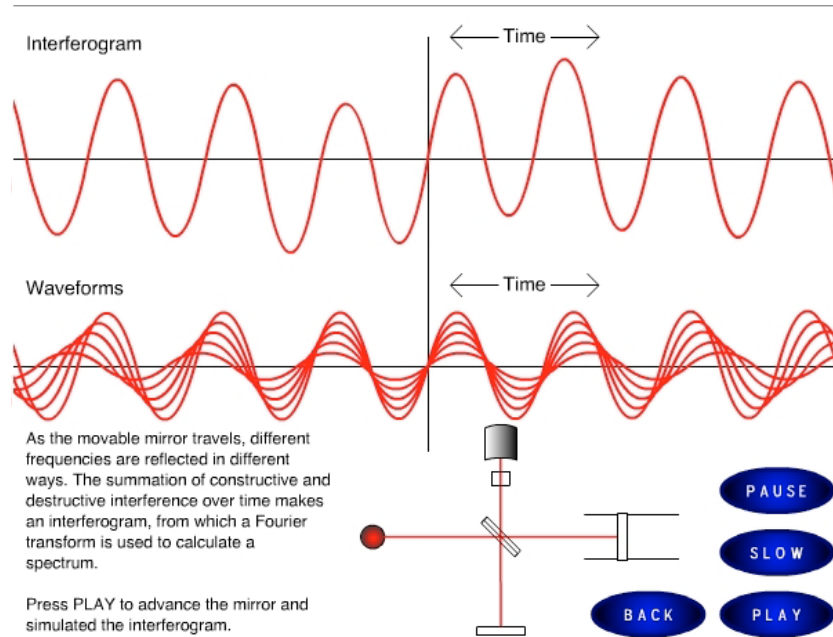
In addition to the vibrations mentioned above, interaction between vibrations can occur (coupling) if the vibrating bonds are joined to a single, central atom. Vibrational coupling is influenced by a number of factors:

- Strong coupling of stretching vibrations occurs when there is a common atom between the two vibrating bonds
- Coupling of bending vibrations occurs when there is a common bond between vibrating groups
- Coupling between a stretching vibration and a bending vibration occurs if the stretching bond is one side of an angle varied by bending vibration
- Coupling is greatest when the coupled groups have approximately equal energies
- No coupling is seen between groups separated by two or more bonds

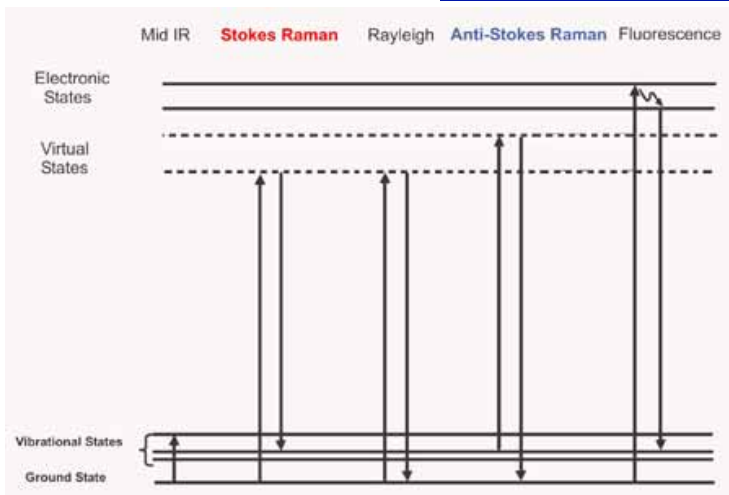
Fourier-Transform IR



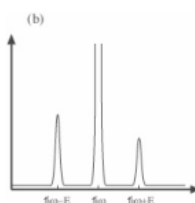
Fourier-Transform IR



Raman basics



Rayleigh scattering: scattering without change of frequency
Stokes Raman (fraction ca. 1×10^{-7}): scattering with lower frequency
Anti-Stokes Raman (weaker still): scattering with higher frequency



(depends on vibrational state of molecule, i.e. certain selection rules apply)

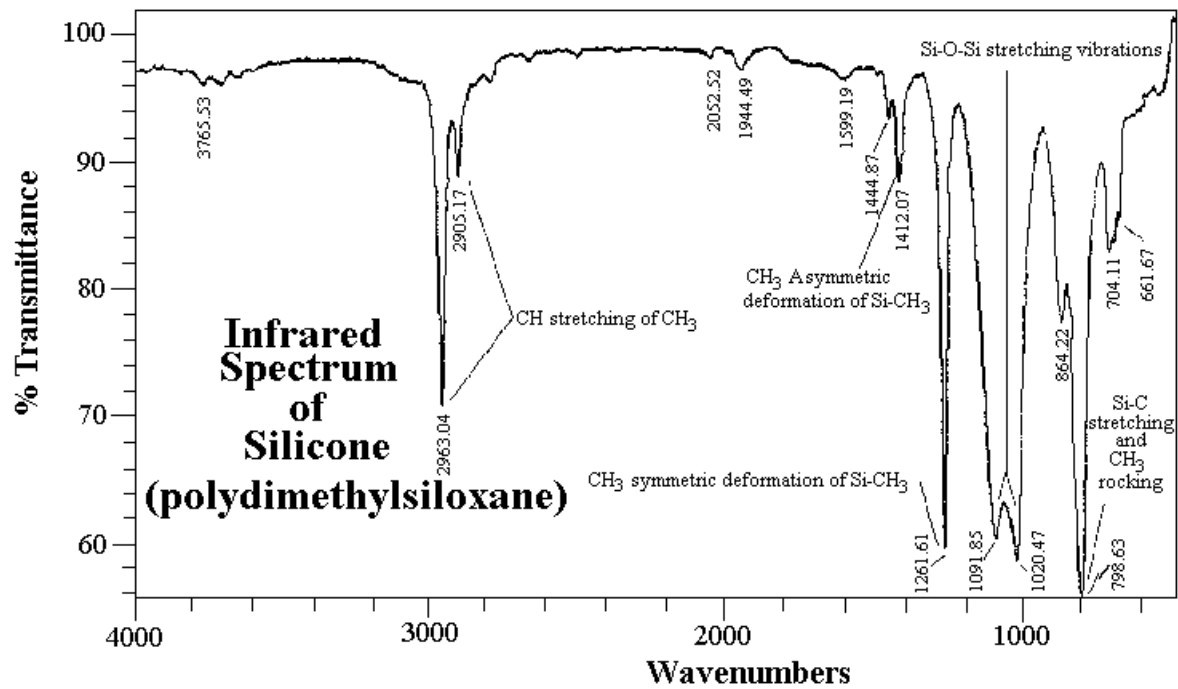
Enhancement of Raman

Resonant Raman - laser wavelength close to absorption wavelength

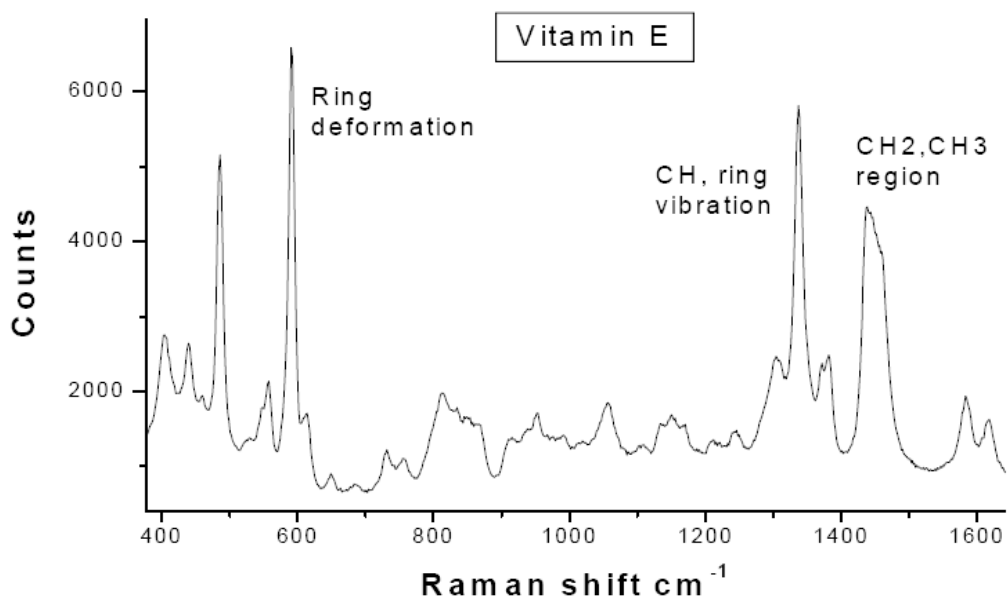
SERS or SERRS (surface enhanced (resonance) Raman spectroscopy) - requires a further moiety to be present (eg. a surface or colloid). The presence of such an agent can provide quite dramatic enhancements and has been used successfully in the study of biological samples such as DNA, peptides and proteins.

Active substrates - a substrate with a special coating that concentrates the sample

Typical IR spectrum



Typical Raman spectrum



Raman spectrum of vitamin E in solution (97%). The spectrum contains several vibrational frequencies each corresponding to certain molecular bonds.
Aquisition time: 30 sec; laser power: 15 mW; confocal Raman microscope

Source: Y. Aksenov, PhD thesis, University of Twente

Bands in IR and Raman spectra of organic molecules

Source: HORIBA Jobin Yvon



Functional Group/ Vibration	Region	Raman	InfraRed
Lattice vibrations in crystals, LA modes	10 - 200 cm^{-1}	strong	strong
$\nu(\text{CC})$ aliphatic chains	250 - 400 cm^{-1}	strong	weak
$\nu(\text{Se-Se})$	290 - 330 cm^{-1}	strong	weak
$\nu(\text{S-S})$	430 - 550 cm^{-1}	strong	weak
$\nu(\text{Si-O-Si})$	450 - 650 cm^{-1}	strong	weak
$\nu(\text{Xmetal-O})$	150 - 450 cm^{-1}	strong	med-weak
$\nu(\text{C-I})$	480 - 660 cm^{-1}	strong	strong
$\nu(\text{C-Br})$	500 - 700 cm^{-1}	strong	strong
$\nu(\text{C-Cl})$	550 - 800 cm^{-1}	strong	strong
$\nu(\text{C-G})$ aliphatic	630 - 790 cm^{-1}	strong	medium
$\nu(\text{C-S})$ aromatic	1080 - 1100 cm^{-1}	strong	medium
$\nu(\text{D-O})$	845 - 900 cm^{-1}	strong	weak
$\nu(\text{C-O-C})$	800 - 970 cm^{-1}	medium	weak
$\nu(\text{C-O-C})$ asym	1060 - 1150 cm^{-1}	weak	strong
$\nu(\text{CC})$ alicyclic, aliphatic chain vibrations	600 - 1300 cm^{-1}	medium	Medium
$\nu(\text{C=S})$	1000 - 1280 cm^{-1}	strong	weak
$\nu(\text{CC})$ aromatic ring chain vibrations	*1580, 1600 cm^{-1}	strong	medium
	*1450, 1500 cm^{-1}	medium	medium
	*1000 cm^{-1}	strong/medium	weak
$\delta(\text{CH}_3)$	1380 cm^{-1}	medium	strong
$\delta(\text{CH}_2)$	1400 - 1470 cm^{-1}	medium	medium
$\delta(\text{CH}_3)$ asym	1400 - 1470 cm^{-1}	medium	medium
$\nu(\text{C-NO}_2)$	1340 - 1380 cm^{-1}	strong	medium
$\nu(\text{C-NO}_2)$ asym	1530 - 1590 cm^{-1}	medium	strong
$\nu(\text{N=N})$ aromatic	1410 - 1440 cm^{-1}	medium	-
$\nu(\text{N=N})$ aliphatic	1550 - 1580 cm^{-1}	medium	-
$\delta(\text{H}_2\text{O})$	~1640 cm^{-1}	weak broad	strong
$\nu(\text{C=N})$	1610 - 1680 cm^{-1}	strong	medium
$\nu(\text{C=C})$	1500 - 1900 cm^{-1}	strong	weak
$\nu(\text{C=O})$	1680 - 1820 cm^{-1}	medium	strong
$\nu(\text{C}\equiv\text{C})$	2100 - 2250 cm^{-1}	strong	weak
$\nu(\text{C}\equiv\text{N})$	2220 - 2255 cm^{-1}	medium	strong
$\nu(\text{S-H})$	2550 - 2600 cm^{-1}	strong	weak
$\nu(\text{C-H})$	2800 - 3000 cm^{-1}	strong	strong
$\nu(\nu(\text{C-H}))$	3000 - 3100 cm^{-1}	strong	medium
$\nu(\nu(\text{C-H}))$	3300 cm^{-1}	weak	strong
$\nu(\text{N-H})$	3300 - 3500 cm^{-1}	medium	medium
$\nu(\text{O-H})$	3100 - 3650 cm^{-1}	weak	strong



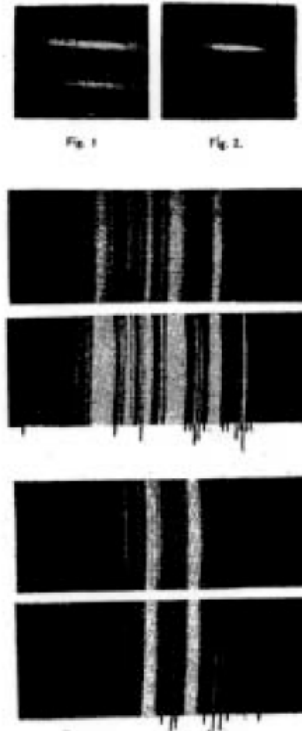
Instrumentation

A few examples

Raman -how it began



Above: Raman's spectrograph with photographic plate
 Right: First spectra published in Indian Journal of Physics

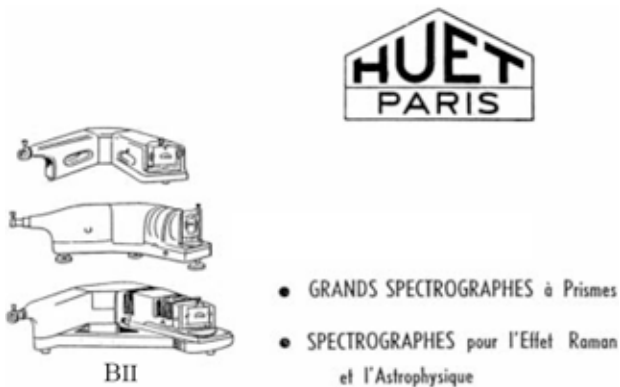


1922-1927: molecular light scattering predictions by Raman, Smekal, Kramers and Heisenberg, Cabannes and Daure, Rocard, and Schroedinger and Dirac

1928: C.V. Raman reports the effect; first he used filtered sunlight, a prism spectroscope, and visual observation, later filtered Hg light and a photographic plate



Spectrometers in the 1940's and 1950's



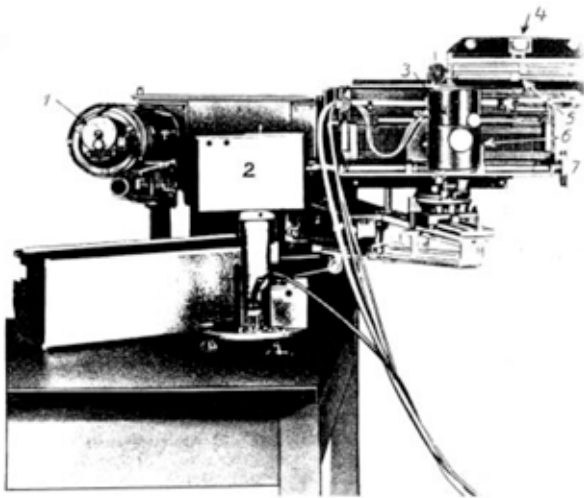
Huet prism (35 cm) spectrograph -1940's



3-4 cm prisms in Steinheil Raman Spectrometer-1957



50 years down the line



Steinheil Raman Spectrometer-1957



Horiba Raman Spectrograph with multiplexing capability for on-line industrial process monitoring-2005



Horiba inverted microscope with Raman Spectrometer-2005



Source: www.jobinyvon.com



University of Twente
The Netherlands



University of Twente
The Netherlands

IR and Raman generated by a chip

InfraRed lasers/LEDs and photodiodes



Photodiode (9 mm size)
(1000-3600 nm)

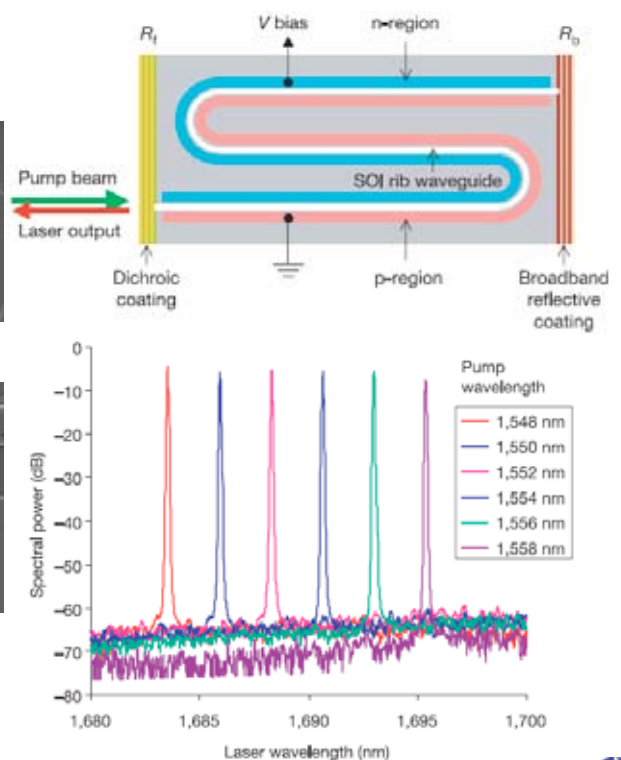
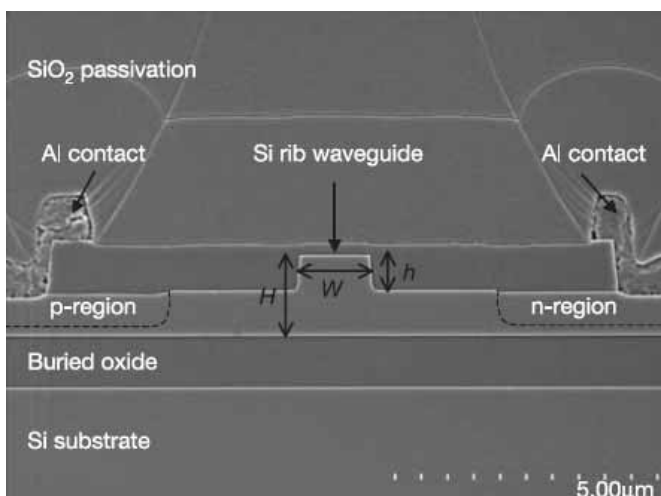


IR laser diode
(735 nm - 3.8 μm)

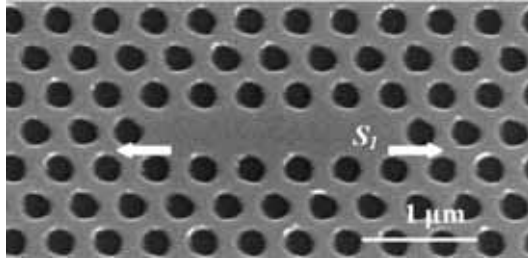
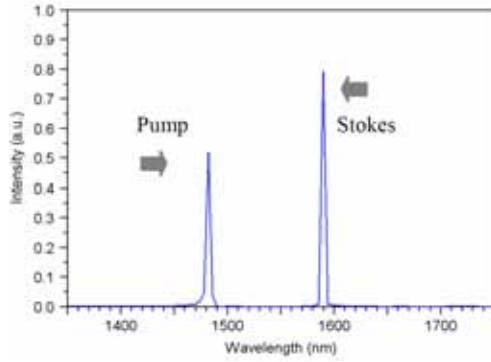


IR LEDs (850 - 940nm)
Sizes 3 -8mm

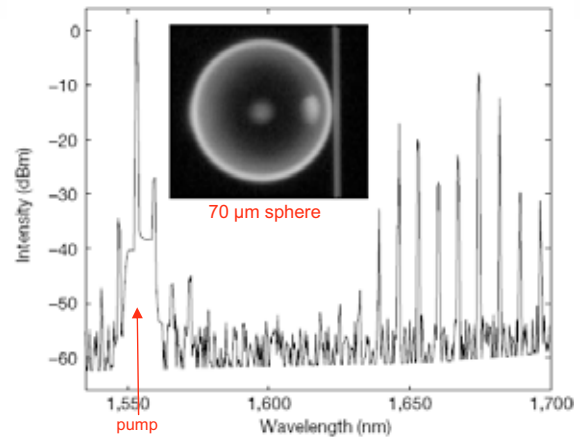
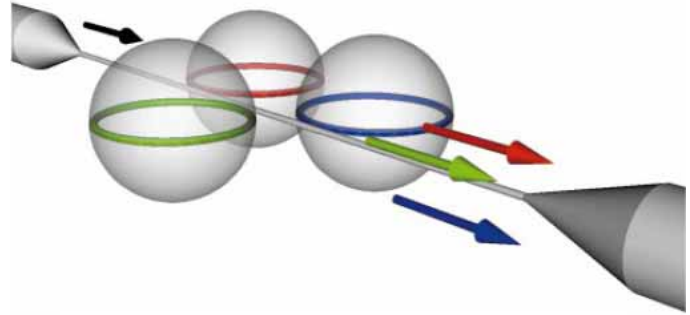
Silicon Raman Lasers



More Raman laser microdevices



Silicon photonic crystal Raman laser
Yang e.a. Optics Express 13, 4723-4730 (2005)

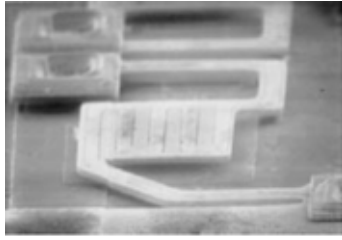


Silica microsphere Raman laser
Spillane e.a Nature 415, 621-623 (2002)

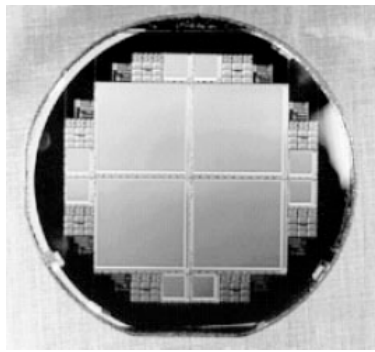
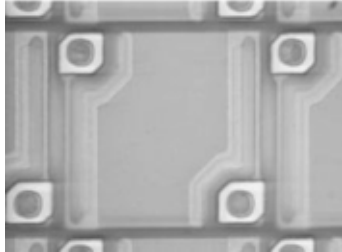


IR and Raman measured by a chip

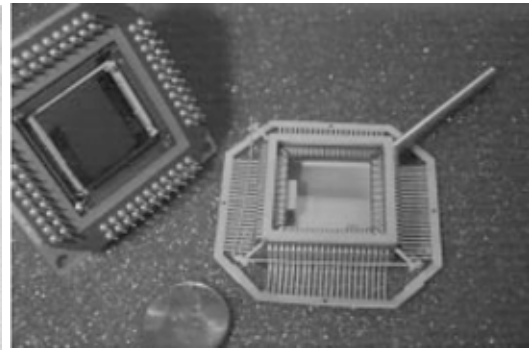
InfraRed detectors



(a)



4" substrate with four 512x512 microemitter pixel arrays



Ceramic vacuum package

Top: microemitter pixel
Bottom: microbolometer (IR-sensor) pixel
Both are on 50 μm pitch



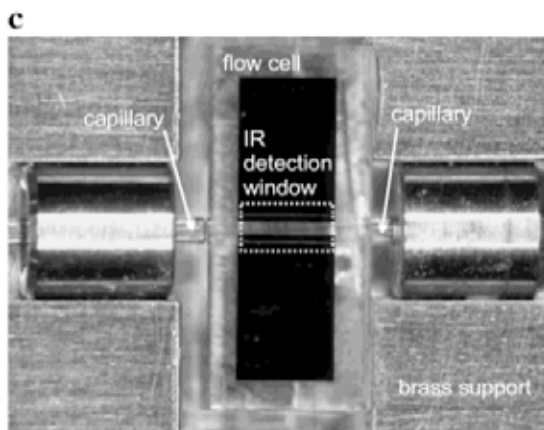
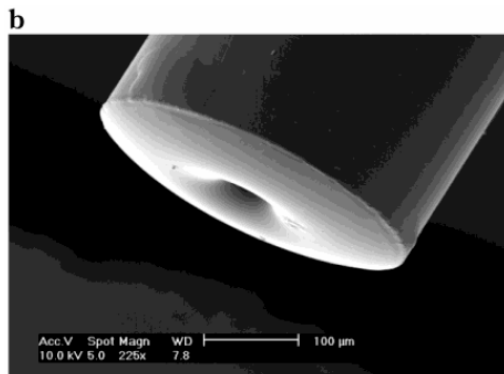
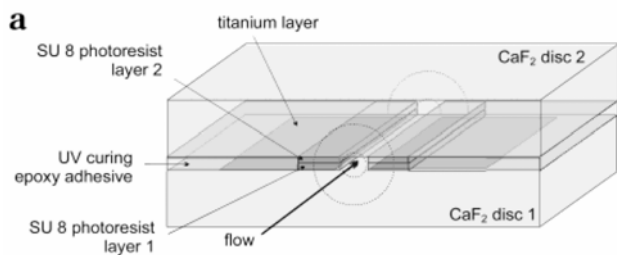
IR image with 240x336 microbolometer camera

Cole e.a. Proc. IEEE 86, 1679-1686 (1998)



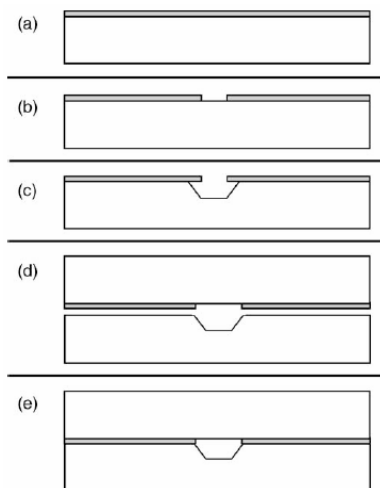
IR and Raman measured on a microfluidic chip

On-line FT-IR detection on CE chips

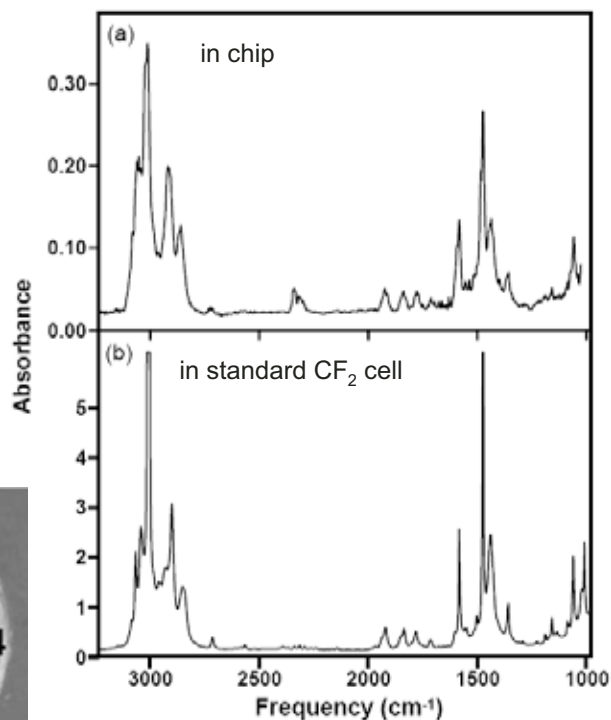
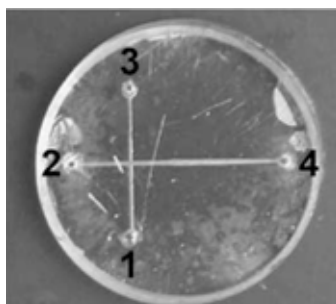


(a) Schematic view of the CE-FT-IR cell
 (b) SEM micrograph of capillary O-ring
 (c) Microscopic view of the CE-FT-IR cell, with connected capillaries, housed in supporting block

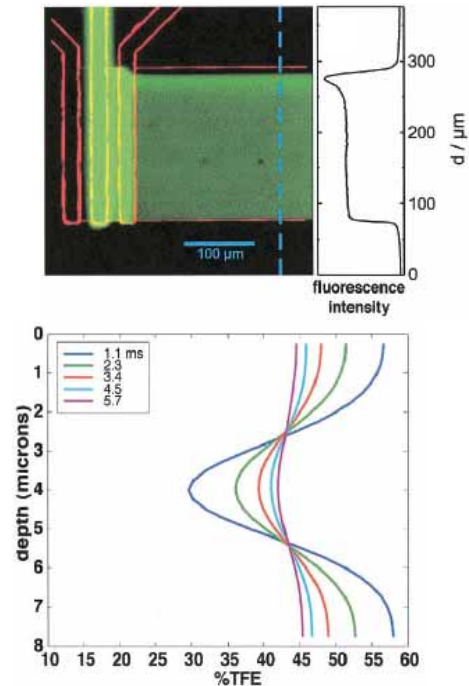
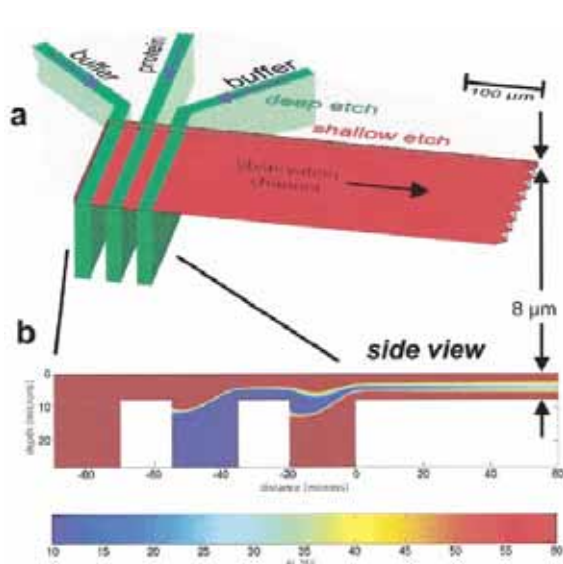
CaF₂ CE chips



etching in saturated aqueous $\text{Fe}(\text{NH}_4)(\text{SO}_4)_2$ solution at $18 \mu\text{m}/\text{day}$; bonding with photoresist (also serves as optical filter), in oven at 135°C for 30 min



Diffusional IR mixer



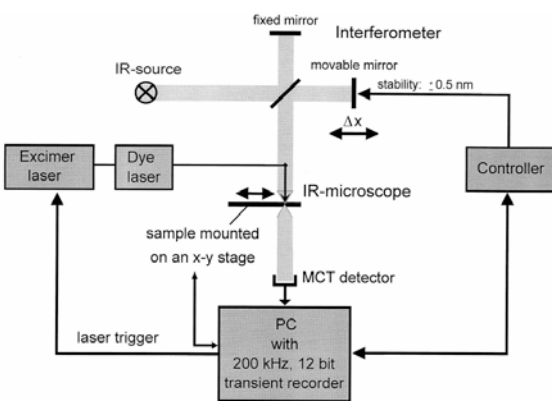
Study of the lifetimes of intermediates in the β -sheet to α -helix transition of β -lactoglobulin; time resolution is achieved by scanning along the observation channel with the focused beam of an FTIR microscope (see next slide)



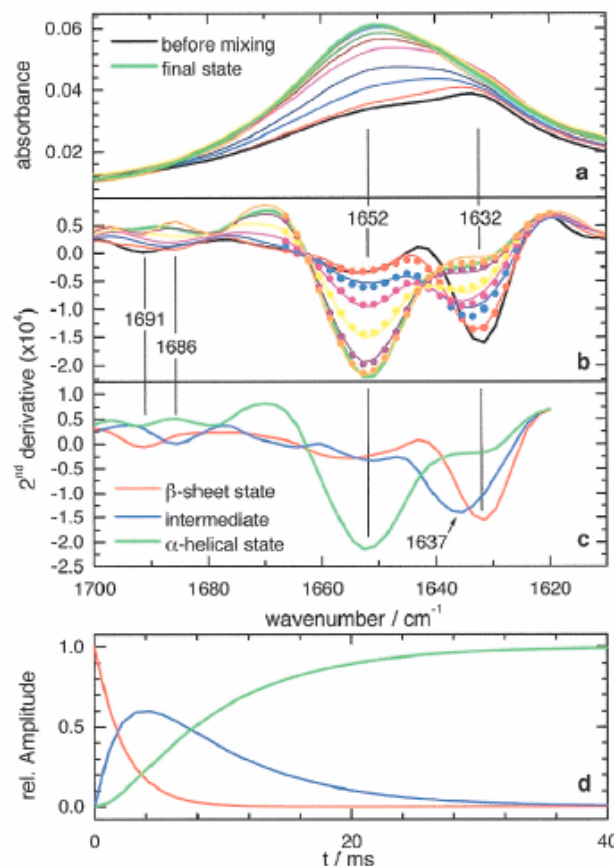
Kauffmann e.a. PNAS 98, 6646-6649 (2001)



FTIR microscope



Rammelsberg e.a. *Vibr.Spectr.* 19, 143-149 (1999)



Time-resolved FTIR spectra and kinetic analysis
 a) spectra taken along the observation channel, at 1.1, 3.4, 5.7, 10.2, 21.6, and 103 ms; black line: before mixing, green line: final state
 b) 2nd derivative spectra of a) with three-state exp. fits (dots); basic spectra are shown in c).
 d) Time course of the 3 states as deduced from the fit

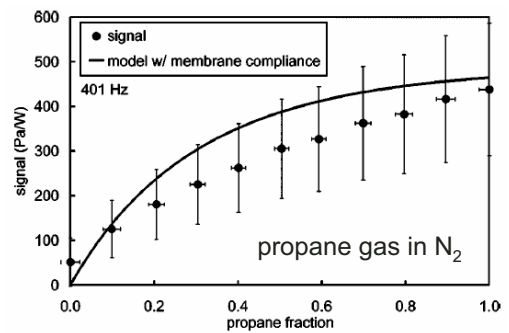
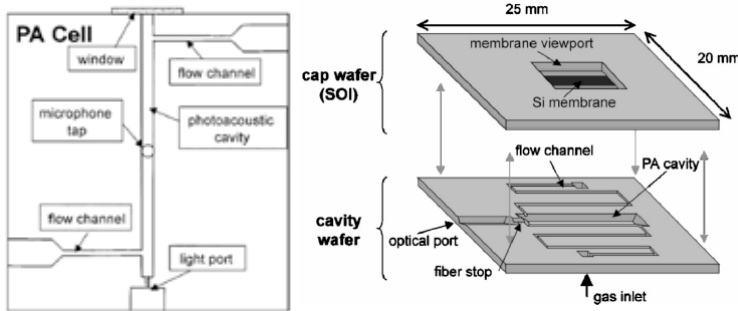
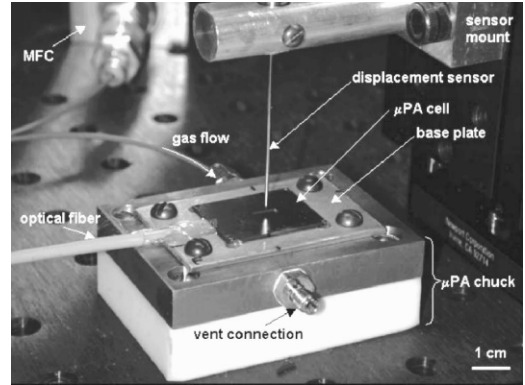
Kauffmann e.a. PNAS 98, 6646-6649 (2001)



Photoacoustic detection on a chip

Principle of photoacoustic spectroscopy:

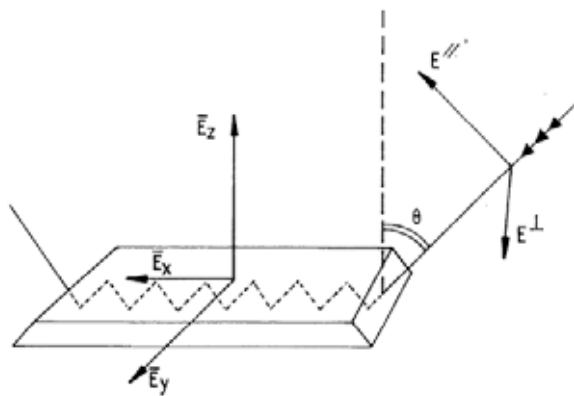
incident light is modulated at an acoustic frequency. If the optical wavelength couples to an energy transition in the gas, the gas absorbs the light resulting in a periodic gas expansion that can be detected by a microphone



Firebaugh e.a. J.Appl.Phys. 92, 1555-1563 (2002)



Attenuated Total (Internal) Reflection



Principle:

IR beam is directed into high refractive index medium which is transparent for IR radiation. Above critical angle θ_c the light beam is completely reflected at the surface. Multiple internal total reflections occur

$$\theta_c = \sin^{-1}\left(\frac{n_2}{n_1}\right)$$

Evanescent wave amplitude:

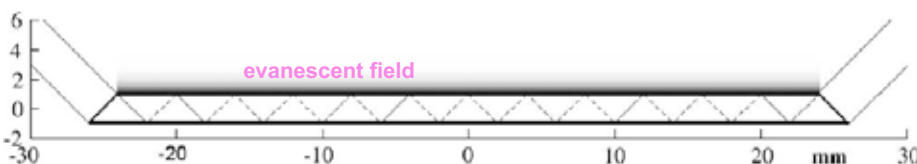
$$E = E_0 \exp\left(\frac{-z}{d_p}\right)$$

Evanescent field penetration depth:

$$d_p = \frac{\lambda}{2\pi n_1 \sqrt{\sin^2 \theta - \left(\frac{n_2}{n_1}\right)^2}}$$

Effective penetration depth for absorbance:

$$d_e = \frac{n_2 E_0^2 d_p}{n_1 \cos \theta}$$



More details in: Vigano e.a. Talanta 65, 1132-1142 (2005)



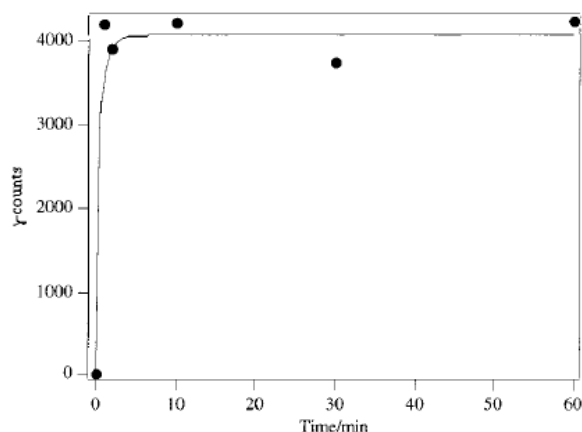
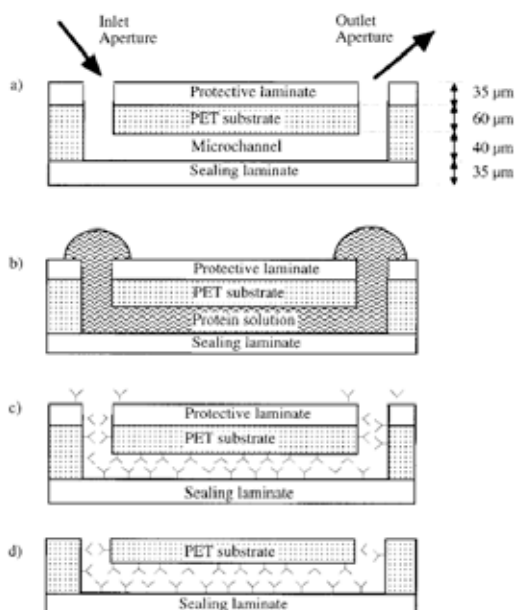
Optical and physical properties of materials

Materials	n_1	θ_c (°) in water	Hardness (kg/mm ²)	Wavelength range	Comments	θ (°)	d_e (μm)	d_p (μm)
Ge	4.0	22	780	4000–830	Stable in water, in acids and alkalis attacked by hot H ₂ SO ₄	30	1.92	0.73
Si	3.4	26	1150	4000–1500	Stable in water, in acids and alkalis attacked by HF and HNO ₃	30	4.32	1.17
						45	1.17	0.51
						60	0.39	0.31
ZnSe	2.4	39	120	4000–650	Stable in water pH 5–9	45	5.29	1.22
						60	1.86	0.67
KRS-5	2.4	39	40	4000–400	Not very stable in water	45	5.29	1.22
						60	1.86	0.67
Diamond	2.35	40	Very hard	4000–400	Stable in water pH 1–14	45	6.17	1.35
						60	2.03	1.69
ZnS	2.2	43	355	4000–950	Stable in water, not at acidic pH	45	12.65	2.34
						60	2.75	0.82

Other materials such as CdTe ($n_1 = 2.65$, hardness = 45) are close to those described in the table. The values of the efficient penetration depth of the evanescent wave have been calculated at a wavelength of 1650 cm^{-1} for a randomly polarized light. The critical angle is calculated in water ($n = 1.5$). KRS-5 is a thallium bromide/thallium iodide eutectic.

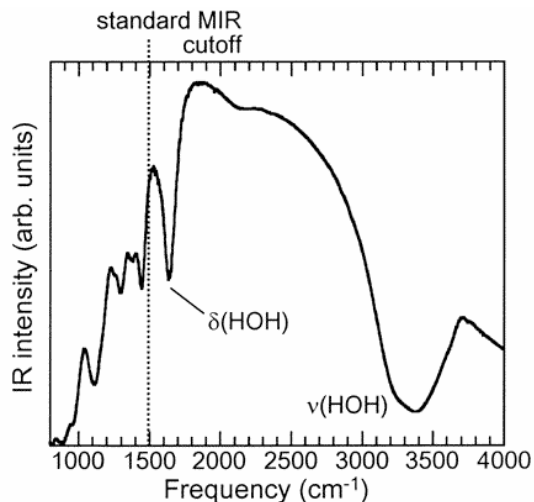
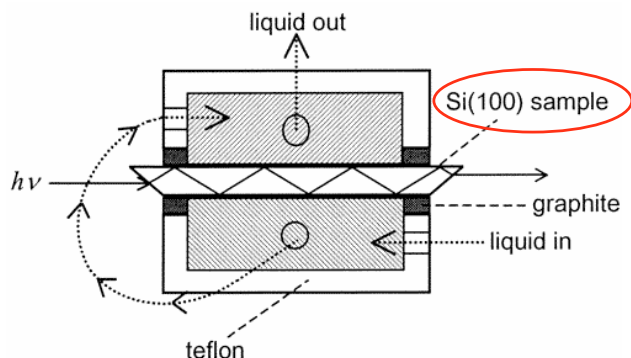
ATR on microchannels

Characterization of Protein Adsorption and Immunosorption Kinetics in Photoablated Polymer Microchannels



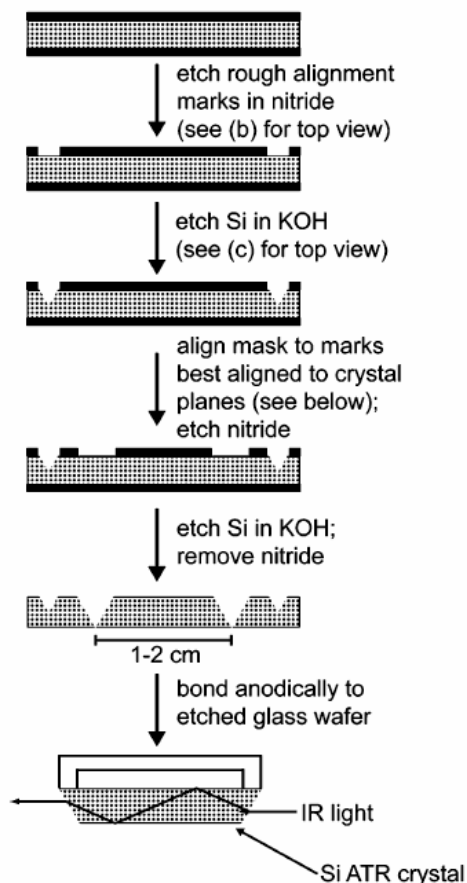
Adsorption kinetics of SEB in a photoablated microchannel. The channel was incubated with 3.12 nM anti-SEB for 1 hr whereas the solution of SEB was incubated at 36 nM between 1 and 60 min and revealed by the secondary radiolabeled anti-SEB at 200 nM.

Extension of IR bandwidth in Si ATR



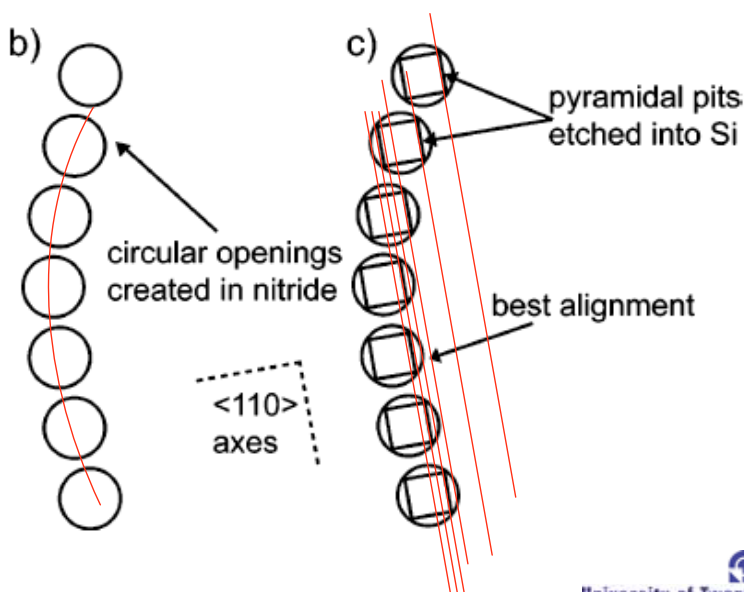
The use of Si(100) allows shorter samples, thus less absorbance in the Si (bandwidth is limited by multiphonon bands that effectively absorb all the incident IR radiation below 1500 cm⁻¹)

NB MIR (Multiple Internal Reflection) = ATR

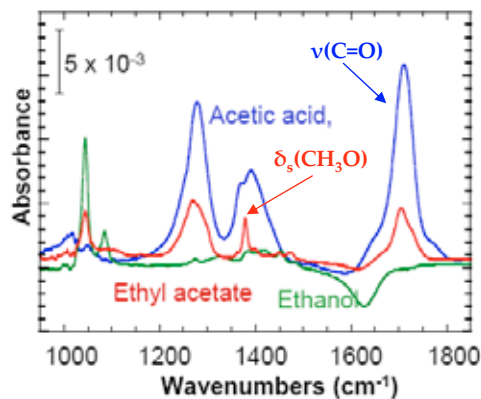
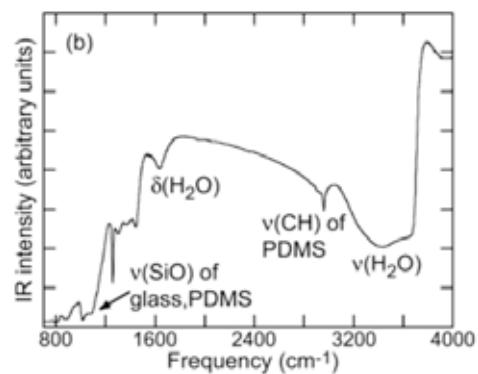
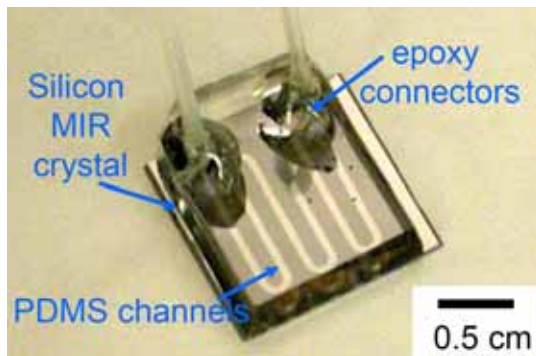


Infrared spectroscopy for chemically specific sensing in silicon-based microreactors

Alignment to <110> directions (needed for ATR inlet aperture)

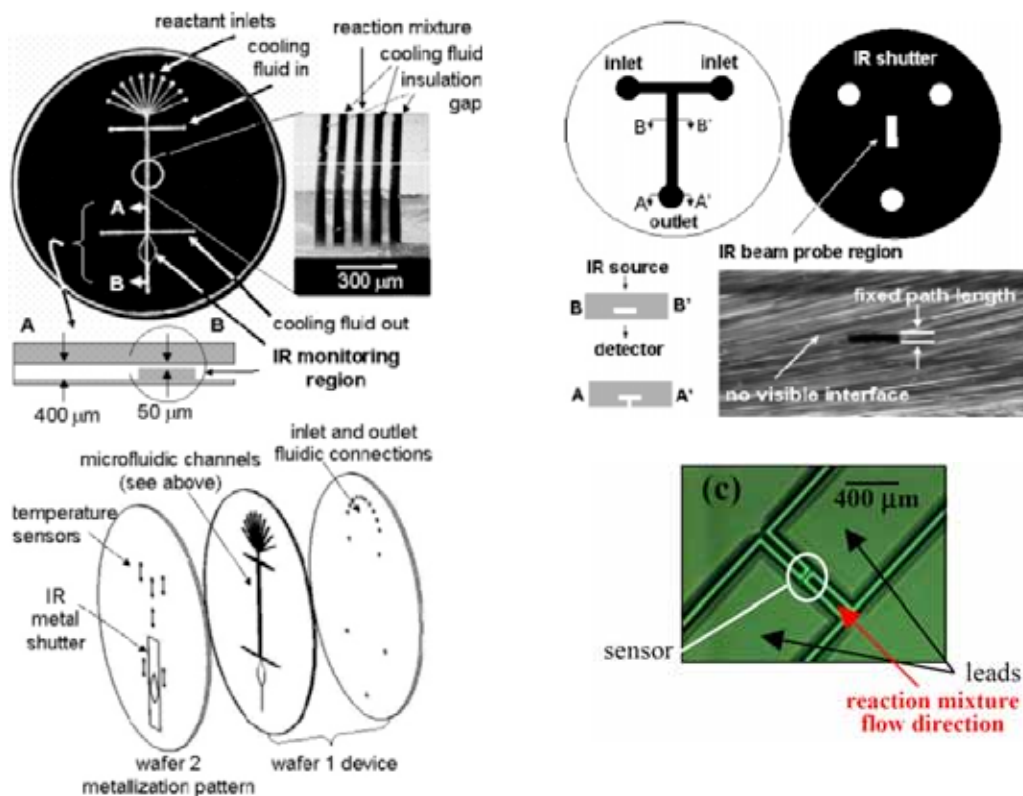


Infrared spectroscopy for chemically specific sensing in silicon-based microreactors

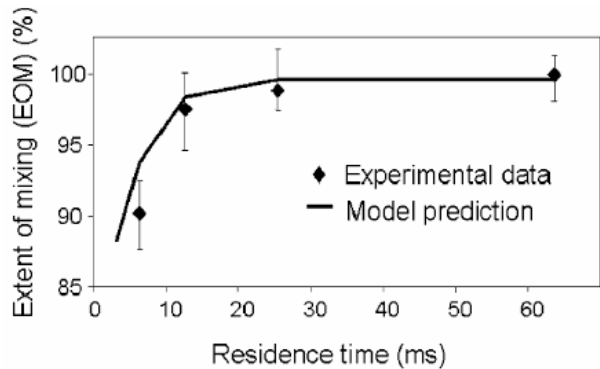
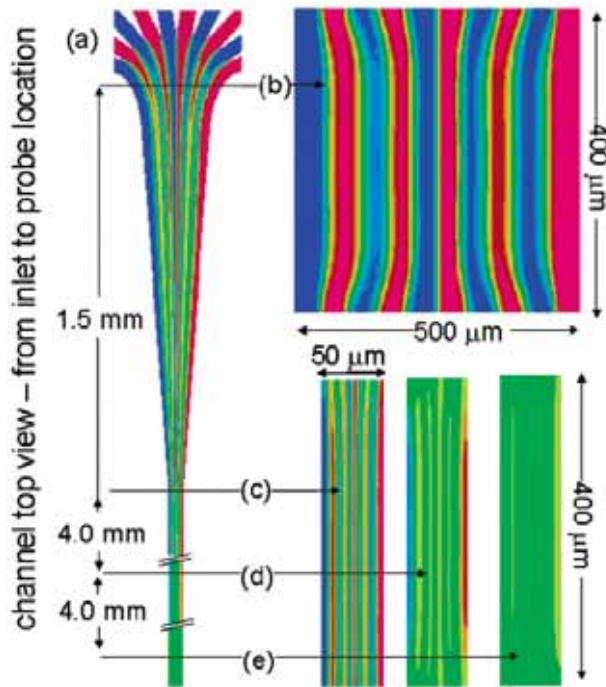


Infrared spectra (100 scans) of reactants and products of ethyl acetate hydrolysis, acquired in aqueous solution (5 ml/100 ml H₂O) in a microreactor

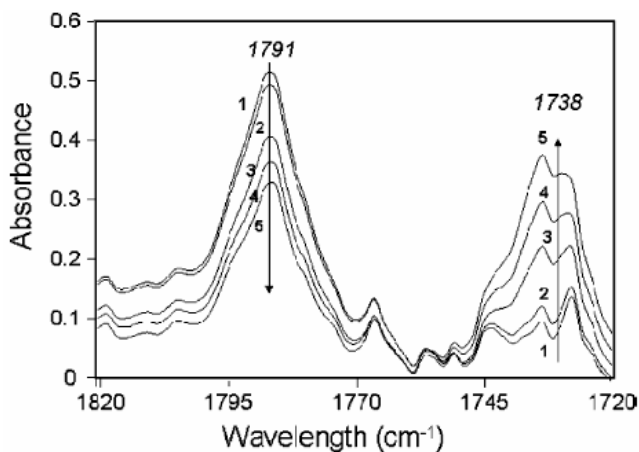
Silicon micromixers with IR detection



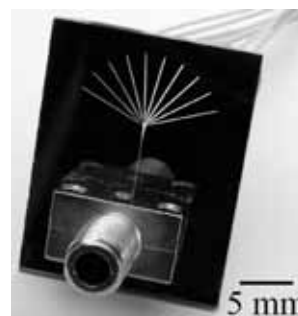
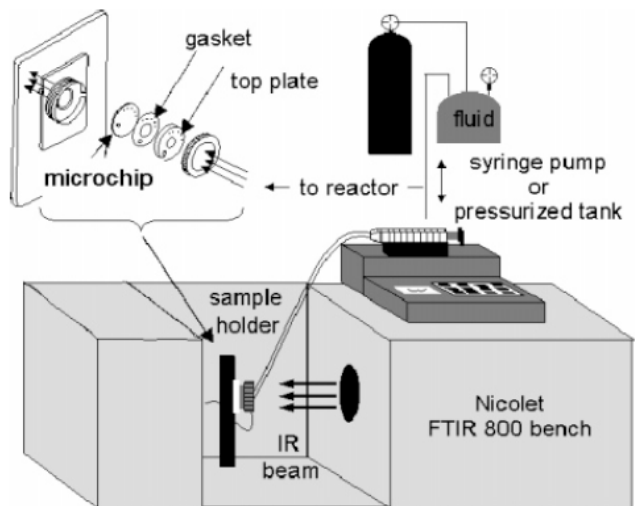
Micromixer simulation and testing



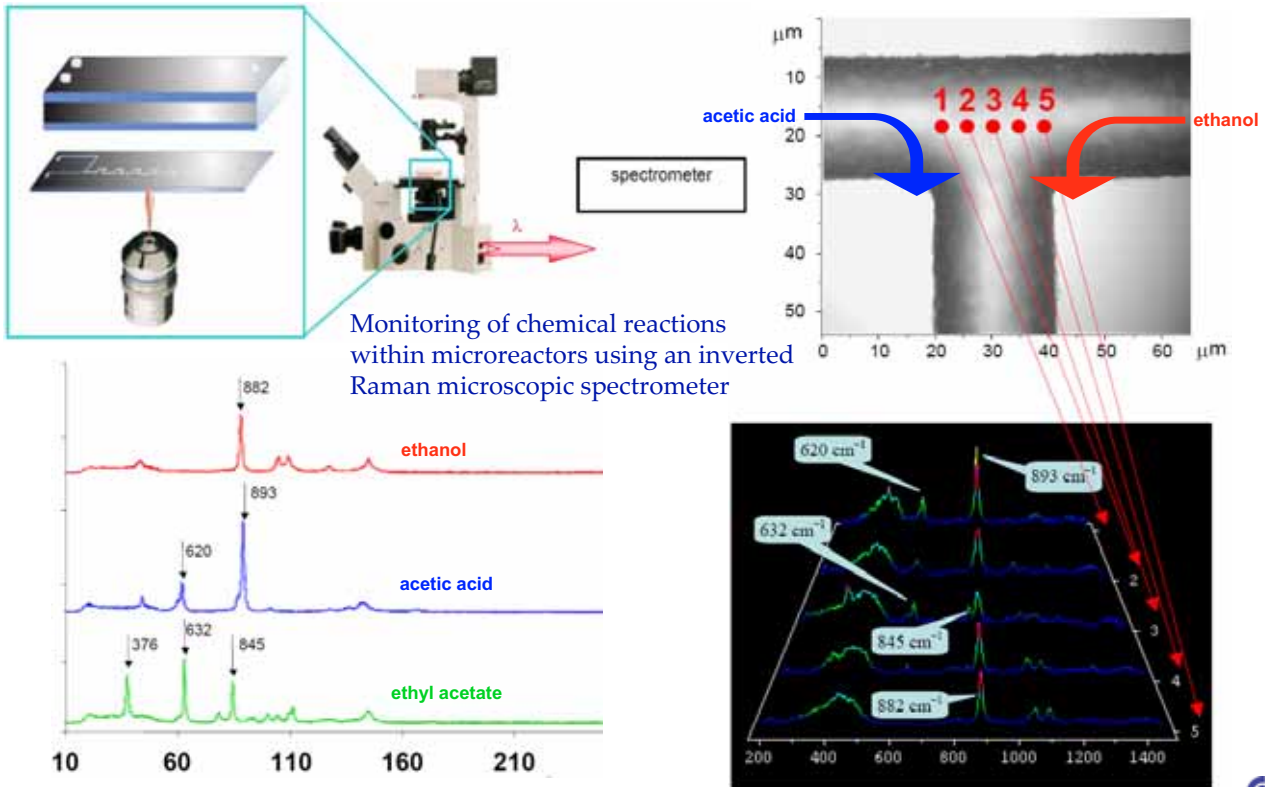
Silicon micromixers with IR detection



FTIR data of the progress of hydrolysis of propionyl chloride: (1) 2.4 s, (2) 4.9 s, (3) 48.6 s, (4) 81 s, and (5) 243 s, 0.4 M propionyl chloride at 23 °C.



Microreactors with Raman microspectrometry

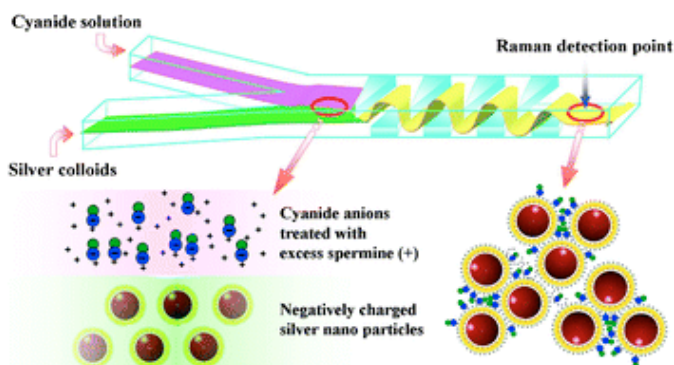


MESA+

Fletcher e.a. Electrophoresis 24, 3239–3245 (2003)

University of Twente
The Netherlands

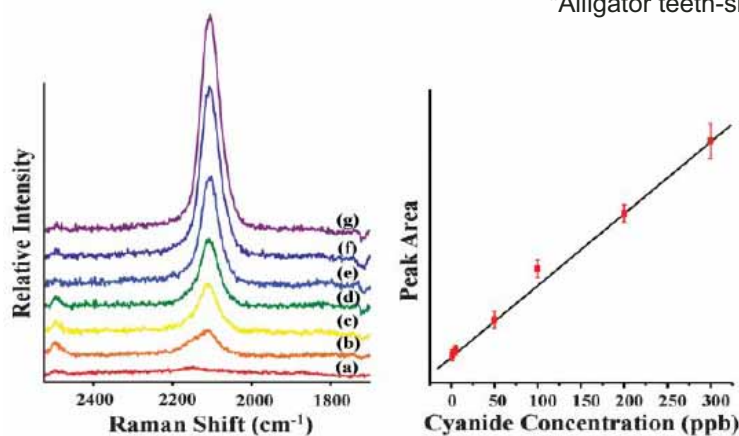
Surface enhanced Raman on a chip



Ultra-sensitive trace analysis of cyanide water pollutant in a PDMS microfluidic channel using confocal surface-enhanced Raman spectroscopy



"Alligator teeth-shaped" microfluidic mixer

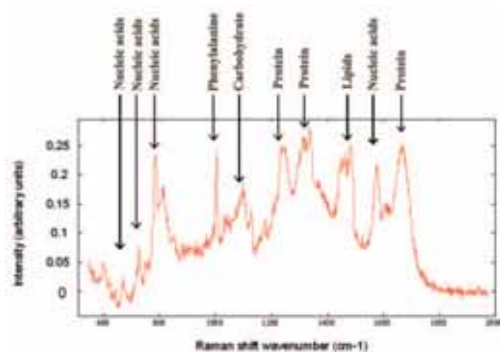


MESA+

Yea e.a. Analyst 130, 1009-1011 (2005) & Lab Chip 5, 437-442 (2005)

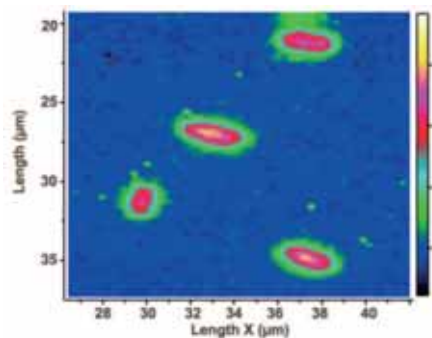
University of Twente
The Netherlands

Raman microspectroscopy on cells

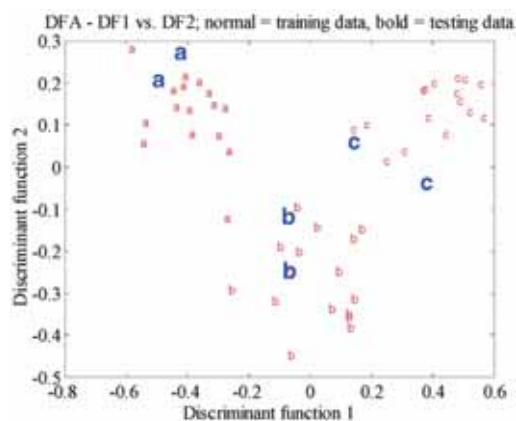


Top left: Typical Raman spectrum acquired from a single cell of size 1-2 μm

Top right: Raman mapped image of four bacteria cells

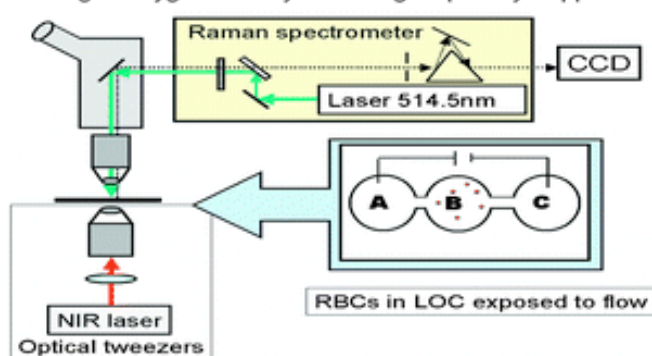


Bottom right: Multivariate analysis of spectra from three bacterial species showing good discrimination between species



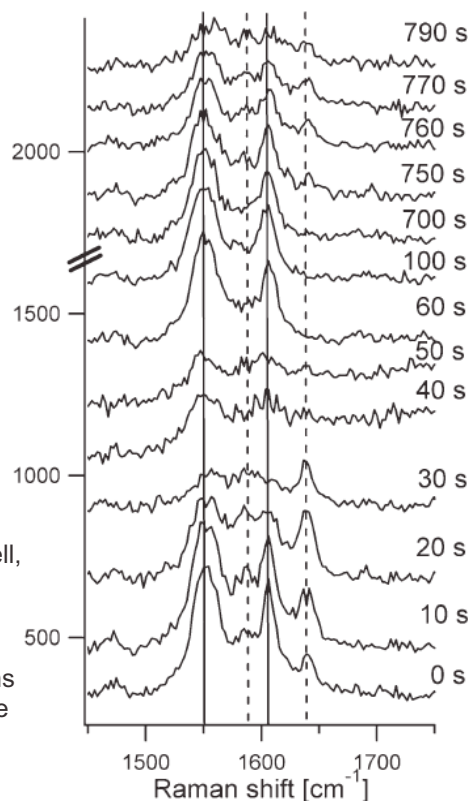
Raman microspectroscopy on cells in a chip

Monitoring of oxygenation cycle in single optically trapped RBCs



Right: Oxygenation cycle of single optically trapped red blood cell, exposed to constant HEPES buffer flow.

After 40 s sodium dithionite is added to chamber A and transported to the RBC through EOF. Next, fresh HEPES buffer was flushed through the reservoir and after ~750 s the RBC turns into a mixed oxy-deoxyHb state again before finally reaching the inactive metHb state after 790 s



Rorschach
inkblot
test

or

InfraRed
image?

